journal

J. Am. Ceram. Soc., 98 [2] 559–566 (2015)
DOI: 10.1111/jace.13325

Relaxor Ferroelectric $BaTiO_3$–$Bi(Mg_{2/3}Nb_{1/3})O_3$ Ceramics for Energy Storage Application

Tong Wang, Li Jin,† Chunchun Li, Qingyuan Hu, and Xiaoyong Wei†

Electronic Materials Research Laboratory, Key Laboratory of the Ministry of Education & International Center for Dielectric Research, Xi'an Jiaotong University, Xi'an 710049, China

Perovskite solid solution ceramics of $(1 - x)BaTiO_3$–$xBi(Mg_{2/3}Nb_{1/3})O_3$ (BT–BMN) ($x = 0.05$–0.2) were synthesized by solid-state reaction technique. The results show that the BMN addition could lower the sintering temperature of BT-based ceramics. X-ray diffraction results reveal a pure perovskite structure for all studied samples. Dielectric measurements exhibit a relaxor-like characteristic for the BT–BMN ceramics, where broadened phase transition peaks change to a temperature-stable permittivity plateau (from −50°C to 300°C) with increasing the BMN content ($x = 0.2$), and slim polarization–electric field hysteresis loops were observed in samples with $x \geq 0.1$. The dielectric breakdown strength and electrical resistivity of BT–BMN ceramics show their maxima of 287.7 kV/cm and 1.53×10^{13} Ω cm at $x = 0.15$, and an energy density of about 1.13 J/cm^3 is achieved in the sample of $x = 0.1$.

I. Introduction

With the fast development of the power electronics, dielectric materials possess high-energy storage density, low loss, and good temperature stability are urgently needed for the potential application in advanced pulsed capacitors.[1–3] To design a proper dielectric material for energy storage application, three requirements have to be satisfied at the same time: large saturated polarization (P_s), small remnant polarization (P_r), and high electric breakdown field strength (BDS).[4] There are four typical kinds of dielectrics for energy storage application: linear dielectric, ferroelectric, relaxor ferroelectric, and antiferroelectric.[5–7] Although, linear dielectrics usually possess higher BDS and lower energy loss, their smaller polarization value (permittivity) makes them not suitable for high-energy storage application, unless the multilayer ceramic capacitors (MLCC) technology is adopt [e.g., $Ca(Zr,Ti)O_3$ and $0.8CaTiO_3$–$0.2CaHfO_3$].[8,9] Ferroelectrics often have larger P_s and moderate BDS, but their larger P_r leads to a smaller energy storage density and lower efficiency.[10] Antiferroelectrics are more likely to be used for high-energy storage because of their larger P_s, smaller P_r and moderate BDS. While most of antiferroelectrics contain environmentally harmful element Pb, such as in $PbZrO_3$[11,12] and $(Pb,La)(Zr,Ti)O_3$[13–15] systems. In recent years due to restriction of the lead-based ferroelectric materials, researchers frequently exploit the environment-friendly lead-free systems.[16] However, the energy storage density of lead-free antiferroelectric ceramics seems not as high as these of lead-based systems. For example, the energy storage density of bismuth-based $0.89Bi_{0.5}Na_{0.5}TiO_3$–$0.06BaTiO_3$–$0.05K_{0.5}Na_{0.5}NbO_3$ antiferroelectric ceramics was rarely larger than 1 J/cm^3.[17,18]

Relaxor ferroelectrics exhibit high P_s, lower P_r and slim hysteresis loop, which makes them promising candidate materials used for the energy storage ceramic capacitors.[19] However, some traditional relaxor ferroelectrics, such as $Pb(Mg_{1/3}Nb_{2/3})O_3$ (PMN)[20,21] and $Pb(Zn_{1/3}Nb_{2/3})O_3$ (PZN),[22,23] are not suitable for energy storage, because of their poor temperature stability. It is urgent to develop new material system for energy storage. Recently, a perovskite-type lead-free relaxor ferroelectric $(1 - x)BaTiO_3$–$xBiScO_3$ (BT–BS)[1,24] system has evoked much interest. For the compositions with appropriate BS content, broadened dielectric peaks correlated to paraelectric–ferroelectric phase transitions gradually transfer into a temperature-independent permittivity plateau accompanying with obvious relaxation characteristics. In addition, the T_{max} (the temperature corresponds to the maximum permittivity ε_{max}) first decreased with the increase in the BS concentration from 120°C for pure BT, and then increased with the increase in the BS content. The change in the T_{max} with composition is in a form of "U" curve. This kind of "U" curve has also been observed in some lead-based and bismuth-based systems, such as $(1 - x)BaTiO_3$–$xBi(Zn_{1/2}Ti_{1/2})O_3$ (BT–BZT),[25] $(1 - x)BaTiO_3$–$xBi(Mg_{1/2}Ti_{1/2})O_3$ (BT–BMT),[26] $(1 - x)BaTiO_3$–$xPb(Zn_{1/3}Nb_{2/3})O_3$ (BT–PZN)[27] and $(1 - x)BaTiO_3$–$xPb(Mg_{1/3}Nb_{2/3})O_3$ (BT–PMN).[28] Due to the limitation of the usage for Pb element, many solid solutions between Bi-based perovskites and BT have been studied, including BT–BS,[1,24] BT–BZT,[25,29–31] and BT–BMT[26,32,33] systems. Among them, BT–BS ceramics[1] showed a ε_{max} of about 1000 at 1 kHz and typical dielectric behavior of relaxor ferroelectric. High-energy storage density has been reported in BT–BS system. BT–BS single-layer capacitor exhibited a ambient temperature energy density of about 6.1 J/cm^3 at a field of 730 kV/cm. BT–BZT ceramic also exhibited dielectric features of relaxor. BT–BMT thin films synthesized by chemical solution deposition displayed stable dielectric properties up to 200°C accompanied with a high-energy density of 37 J/cm^3 at 1900 kV/cm at ambient temperature.[33] The energy density of about 6.1 J/cm^3 (BT–BS) and 37 J/cm^3 (BT–BMT) were obtained by MLCC technology and thin film processing, respectively. The overall stored energy of thin films is still small due to their thin thickness limitation and do not meet the requirement in some cases. Furthermore, the energy storage density of bulk ceramics for BT–BS, BT–BMT, and BT–BZT were around from 1 to 2 J/cm^3. However, there is no report on $BaTiO_3$–$Bi(Mg_{2/3}Nb_{1/3})O_3$ (BT–BMN) system. Hong *et al.* reported a high T_C and typical dielectric features in relaxor ferroelectric $PbTiO_3$–$Bi(Mg_{2/3}Nb_{1/3})O_3$ solid solution.[34] Therefore, it is highly possible that the BT–BMN system exhibit similar features like that of BT–BS, BT–BZT, and BT–BMT systems.

In this study, we focused on the dielectric behaviors of relaxor ferroelectric $BaTiO_3$–$Bi(Mg_{2/3}Nb_{1/3})O_3$ ceramics. The effects of BMN content on processing, microstructures, and dielectric properties of the BT–BMN system were

D. Lupascu—contributing editor

Manuscript No. 34925. Received April 29, 2014; approved October 11, 2014.
†Author to whom correspondence should be addressed. e-mails: ljin@mail.xjtu.edu.cn, wdy@mail.xjtu.edu.cn

systematically investigated. Finally, the energy storage properties were evaluated from the point view of applications.

II. Experimental Procedure

(1) Sample Preparation

ABO_3 perovskite structure dense $(1-x)BaTiO_3$–$xBi(Mg_{2/3}Nb_{1/3})O_3$ ($x = 0.05$, 0.1, 0.15, 0.2) (BTBMN1–4) ceramics were prepared by conventional solid-state reactions from analytical reagent grade powders of $BaCO_3$, TiO_2, Bi_2O_3, MgO, and Nb_2O_5 (AR, Beijing Sinopharm chemical reagent Co. Ltd., Beijing, China). The initial raw powders were mixed and ball-milled using zirconia balls for 6 h in polyethylene jars with ethanol as media. After drying, the mixture was calcined at 1100°C for 2 h in a covered alumina crucible to prevent the volatilization of bismuth oxide. The calcined powders were re-milled, mixed with 5 wt% solution of PVA as a binder, and uniaxially pressed into cylindrical disks under a pressure of 150 MPa with 12 mm in diameter and 1–2 mm in thickness. The samples were fired at 600°C for 4 h to remove the organic binder and then sintered in a covered alumina crucible at 1150°C–1350°C for 2 h to restrain the volatilization of bismuth.

(2) Sample Characterization

The densities of the sintered ceramics were measured by Archimedes method. The phase structures of the sintered ceramics were examined using an X-ray diffractometer (XRD, Rigaku D/MAX-2400, Tokyo, Japan) using CuK_α radiation ($\lambda = 0.15406$ nm) operating at 40 kV and 100 mA. The microstructure of the ceramic samples was observed using scanning electron microscopy (SEM, FEI Quanta 250 FEG, Hillsboro, OR). For electrical measurements, the sintered pellets were polished to achieve parallel and smooth faces, and gold electrodes were sputtered on both faces. The temperature dependence of permittivity and loss tangent were carried out from −180°C to 600°C in custom-designed furnaces with a precision LCR meter (E4980A; Agilent, Palo Alto, CA) over a frequency range from 100 Hz to 1 MHz. The real (Z') and imaginary (Z'') parts of the complex impedance were determined by an Agilent E4980A LCR meter from 100 Hz to 1 MHz. The DC resistivity was acquired using a high resistance meter (4339A, HP, Palo Alto, CA) at ambient temperature. Dielectric breakdown strength (BDS) of the samples was determined at ambient temperature using a high voltage source (HF5013K; Huiyou Electronics Co. Ltd., Chang Zhou, China). Circular specimens with 0.3–0.5 mm in thickness were tested in silicon oil to prevent arcing. At least 10 specimens were used for the BDS testing. The polarization–electric field (P–E) hysteresis loops were measured at ambient temperature at 10 Hz using a ferroelectric test system (TF Analyzer 2000; aixACCT, Aachen, Germany).

III. Results and Discussion

Figure 1 shows the relationships between sintering temperatures and densities of all studied samples. It can be observed that increasing the BMN content could decrease the sintering temperature while increase the density. Figure 2(a) shows the XRD patterns of BT–BMN ceramics with various amounts of BMN. The XRD results suggest a pure perovskite structure without any detectable second phase. The peaks were indexed using a powder diffraction file (PDF) with No.792263. In addition, no peak splitting for the (200) peak was detected in Fig. 2(b). Therefore, it seems that the reflection peaks of BT–BMN ceramics could be indexed as a pseudocubic symmetry. With the increase in BMN content, diffraction peaks gradually shift toward lower degree [Fig. 2(b)]. This phenomenon indicates that the interplanar

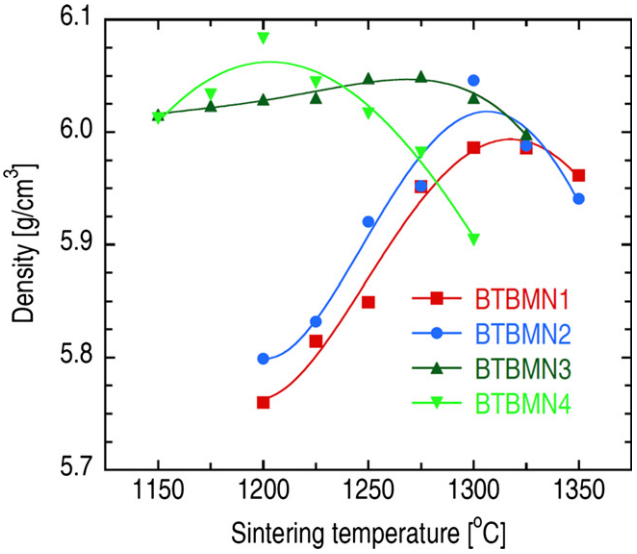

Fig. 1. The density of BT–BMN ceramics as a function of sintering temperature for 2 h. The sold lines are a guide for the eye.

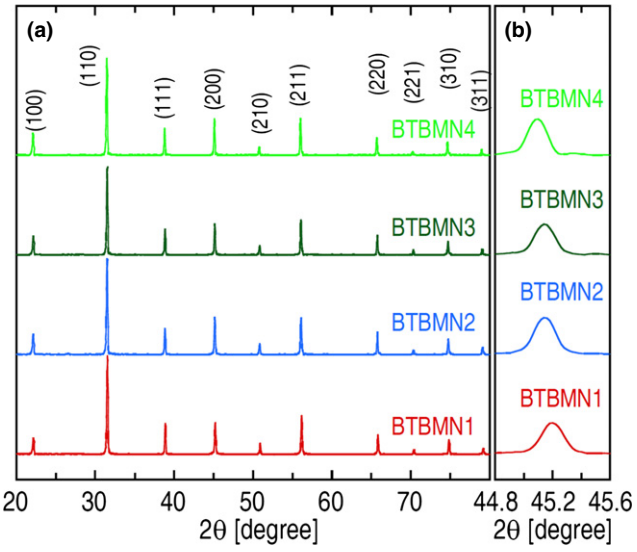

Fig. 2. (a) XRD patterns of BT–BMN ceramics; (b) enlarged XRD patterns from 44.8° to 45.6°of BT–BMN ceramics.

spacing becomes wider. The lattice parameters are listed in Table I.

As the concentration of BMN increased, the unit cell volume increased. Bi^{3+} (1.11 Å) is slightly smaller than Ba^{2+} (1.61 Å) owing to 12-fold coordination in A-site,[26] whereas the B-site ion Mg^{2+} (0.72 Å) and Nb^{5+} (0.64 Å) have lager radius than that of Ti^{4+} (0.604 Å) (sixfold coordination).[26,35] A tolerance factor between 0.79 and 1.1 gives an ideal perovskite structure.[36] The equivalent ionic radii of Mg^{2+} and Nb^{5+} ions can be calculated by the following equation: $r = \frac{2}{3}r(Mg^{2+}) + \frac{1}{3}r(Nb^{5+}) = 0.693$Å (ionic radii for $Mg^{2+} = 0.72$ Å, and $Nb^{5+} = 0.64$ Å). The tolerance factor of Mg^{2+} and Nb^{5+} ions substitution of A site and B site are 0.739 and 1.017, respectively. The equivalent ionic radii of Mg^{2+} and Nb^{5+} are much smaller than that of Ba^{2+} (1.61 Å). Moreover, the tolerance factor of Bi^{3+} ions substitution of A site and B site are 0.886 and 0.848, respectively. The Bi^{3+} is much larger than that of Ti^{4+} (0.604 Å). It is believed that Mg^{2+} and Nb^{5+} ions were more likely to enter the B-site substituting Ti^{4+}, and Bi^{3+} ions was more likely

Table I. The Lattice Parameters for BT–BMN Ceramics

Sample	BTBMN1	BTBMN2	BTBMN3	BTBMN4
a (Å)	4.009	4.013	4.014	4.017
b (Å)	4.009	4.013	4.014	4.017
c (Å)	4.009	4.013	4.014	4.017
Cell volume (Å^3)	64.433	64.626	64.674	64.819

to enter the A-site substituting Ba^{2+}. The cell volume (see Table I) increased with increasing the BMN content, indicating that in the BT–BMN perovskite structure the B-O_6 octahedra dominate the unit cell volume.

SEM micrographs of the thermally etched surfaces for BT–BMN ceramics are shown in Fig. 3. No significant differences can be found among these four images. The grain size increased slightly with the concentration of BTBMN. This result indicates that BMN could promote the densification of BT–BMN ceramics.

Figure 4 shows the temperature dependence of permittivity and dielectric loss tangent for BT–BMT ceramics measured at different frequencies from −180°C to 300°C. Because of the equipment limitation, this picture consisted of two parts of data (from −180°C to 160°C and from ambient temperature to 600°C). BT–BMN ceramics exhibited a significant frequency dispersion of the dielectric permittivity and dielectric loss, implying a relaxor characterization. Moreover, broadened phase transition peaks change to a temperature-stable permittivity plateau (permittivity from 628 to 787 with temperature from −50°C to 300°C at 1 kHz) with increasing BMN content (x = 0.2). As shown in Fig. 4(d), the permittivity change with temperature for BTBTM4 ceramics are less than ±12% over the temperature range from −55°C to 125°C at 100 Hz. The emergence of the relaxor behavior caused by the addition of BMN in the BT ceramics is in accord with the assumptions by Setter *et al.*[37] and Bokov *et al.*[38] According to their assumptions, the large differences in valence between the B′ and B″ ions, or small size of A-site cation would enhance elastic drive toward ordering on the B site. Large size differences in B-site cations are driven strongly toward ordering by electric forces in $A(B'B'')O_3$ system. The diffuse transition would be sharpened by the increase in B-site cations ordering. In our study, it can be seen that Bi^{3+} has smaller radius than Ba^{2+} in A site, whereas Mg^{2+} and Nb^{5+} have large radii than Ti^{4+} in B site, which would cause relaxor behavior in the BT–BMN system.

For further comparison of relaxation quantitatively, ΔT_m have been introduced. The ΔT_m used to characterize the degree of frequency dispersion in the frequency range from 100 Hz to 1 MHz is defined as follows:[39]

$$\Delta T_m = T_{m(1\ MHz)} - T_{m(100\ Hz)} \quad (1)$$

where $T_{m(1\ MHz)}$ and $T_{m(100\ Hz)}$ are the temperature at the peak of the permittivity measured at 1 MHz and 100 Hz, respectively. The values of ΔT_m are 44°C, 80°C, 88°C, and 115°C, for BTBMN1, BTBMN2, BTBMN3, and BTBMN4, respectively. In general, relaxor feature appears when at least two cations occupy the same crystallographic lattice site, either in A site or B site, which gives rise to random fields that impede the development of long-range polar ordering. In this work, the substitution of the Ba^{2+} by Bi^{3+} and Ti^{4+} by Mg^{2+} and Nb^{5+} enhance the positional disorder in A- and B-site ions of ABO_3 perovskite, accordingly, resulting in the increase in relaxor behavior.

Table II summarizes T_m, ε_{max}, permittivity (ε_{RT}), and dielectric loss tangent ($\tan\delta_{RT}$) at ambient temperature measured at 100 kHz. It can be seen that the ε_{max} and ambient temperature permittivity of BT–BMN ceramics decreases with increasing BMN content. T_m of BT–BMN ceramics increases with increasing BMN content. The increase in T_m with $Bi(Me'Me'')O_3$ concentration is also observed within a pseudocubic phase region for BT–BS, BT–BZT, and BT–BMT systems.[24,29,32] Figure 5 shows the dielectric permittivity as the function of temperature of BTBMN ceramics

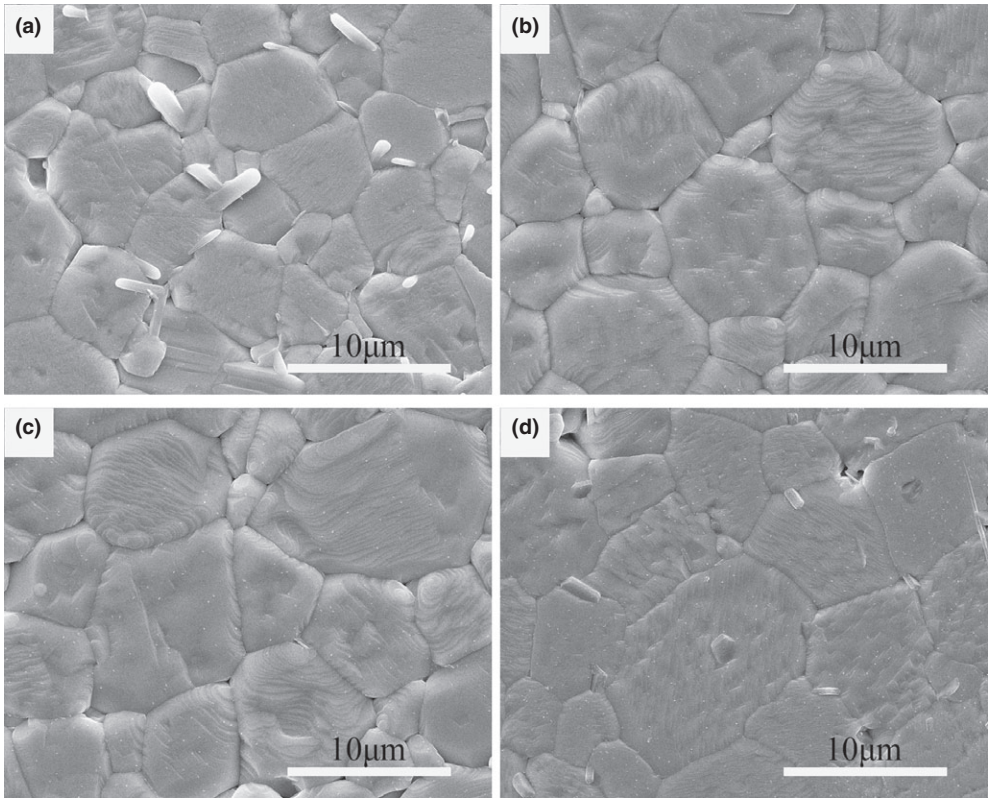

Fig. 3. SEM images of the thermally etched surfaces of the BT–BMN ceramics: (a) BTBMN1; (b) BTBMN2; (c) BTBMN3; (d) BTBMN4. Thermal etching was performed at 100°C below the sintering temperature of BT–BMN ceramics for 30 min.

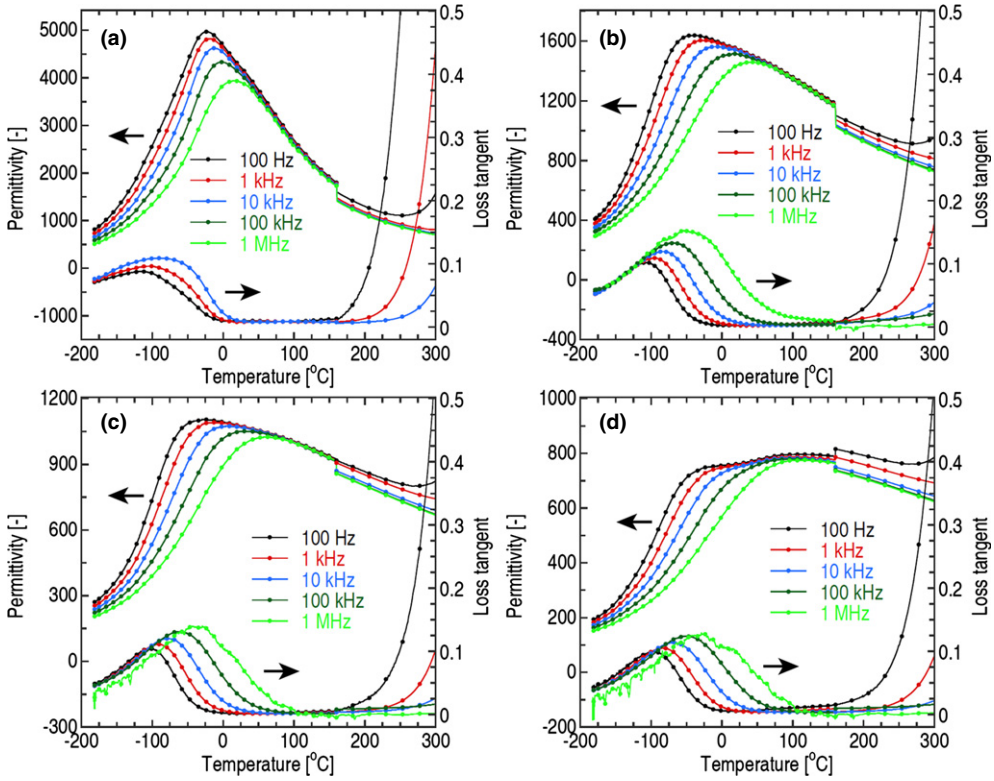

Fig. 4. Temperature dependence of permittivity and loss tangent of (a) BTBMN1; (b) BTBMN2; (c) BTBMN3; and (d) BTBMN4 ceramics measured from −180°C to 300°C. The data from −180°C to 160°C were measured by a low-temperature dielectric spectrum system, whereas the data from 160°C to 300°C were collected by another high-temperature dielectric spectrum system. Therefore, the jump shown in Fig. 4 at 160°C is due to the connection of these two sets of data, instead of an indication of dielectric abnormal.

measured at different frequencies from room temperature to 600°C. Of particular interest is the flat temperature coefficient of capacitance in the temperature range of ambient temperature to 300°C, exhibiting good temperature stability.

Impedance spectroscopy has been accepted as a powerful experimental technique to separate the contribution from grain, grain boundary, and interfaces.[30,40–44] Figure 6 shows the complex impedance plane plots (Z''–Z') measured at 500°C for BT–BMN ceramics. All samples showed an electrical inhomogeneity character by two semicircles. One is at low-frequency range, whereas the other one is at high-frequency range. All the data were fitted based on an equivalent circuit, which is composed by two parallel R (resistor) and CPE (constant phase element) units connected in series.[40–44] The capacitance value corresponding to the low-frequency arc is in the range 49–198 nF. The high-frequency arc has a smaller capacitance value around 338–748 pF. According to the relationship established by Irvine *et al.*,[45] the high frequency corresponds to the response of grain, and the low frequency corresponds to the response of grain boundary. In addition, it is easily seen from Fig. 6 that both the grain and the grain-boundary resistance increase with the increase in BMN concentration. The portion of grain impedance becomes larger systematically from the comparison of radii between the grain and the grain-boundary impedance.

Table II. Dielectric Properties of BT–BMN Ceramics at 100 kHz

Sample	T_m (°C)	ε_{max}	ε_{RT}	$\tan\delta_{RT}$
BTBMN1	−2	4332	4068	0.028
BTBMN2	14	1516	1509	0.022
BTBMN3	32	1051	1050	0.027
BTBMN4	98	779	726	0.045

In special temperature, the equivalent circuit is reduced to a combined R_g (grain) and C_{gb} (grain boundary) connected in series. This will give rise to a Debye-like relaxation. The peak frequency is inversely proportional to R_gC_{gb}. A similar result was reported on the relaxor-like behavior in $CaCu_3Ti_4O_{12}$ ceramics.[40] The frequency values were calculated using Eq. (2):[44]

$$\omega\tau = \omega RC = 2\pi fRC = 1 \quad (2)$$

where ω is the frequency and τ the relaxation time. The characteristic frequency caused by R_g and C_{gb} of BTBMN ceramics is in the range 0.2–0.9 kHz. It is worth noting that the dielectric relaxation in Fig. 5 appears at around 500°C when the frequency was 1 kHz. This implies that the observed dielectric relaxation is closely related to the interfacial polarization taking place between the bulk and the grain boundary.

Figure 7 shows the Weibull distribution,[46–48] which is usually used for the BDS analysis, of the dielectric BDS for BTBMN ceramics with different BMN contents. When $m > 1$, it indicates that the failure could be analyzed by the Weibull model.[49–51] The value of the Weibull modulus m was obtained by linear fitting of the experimental data and presented in Fig. 7. The value of BDS was obtained from the intercept of each line and plotted in the inset of Fig. 7. The average BDS value showed a maximum 287.7 kV/cm at $x = 0.15$. It is well known that dielectric ceramics with higher density usually exhibit higher BDS. Therefore, it is believed that the improvement of BDS is attributed to the increase in density with increasing the BMN content. The result coincide with others reported the BDS increased with the increasing ceramics density in $BaTiO_3$ and $(Ba,Sr)TiO_3$ ceramics.[52–54] Moreover, the decreases in permittivity with increasing BMN content, which indicate the substantial breakdown of long-range dipole interaction by incorporation of BMN. It was

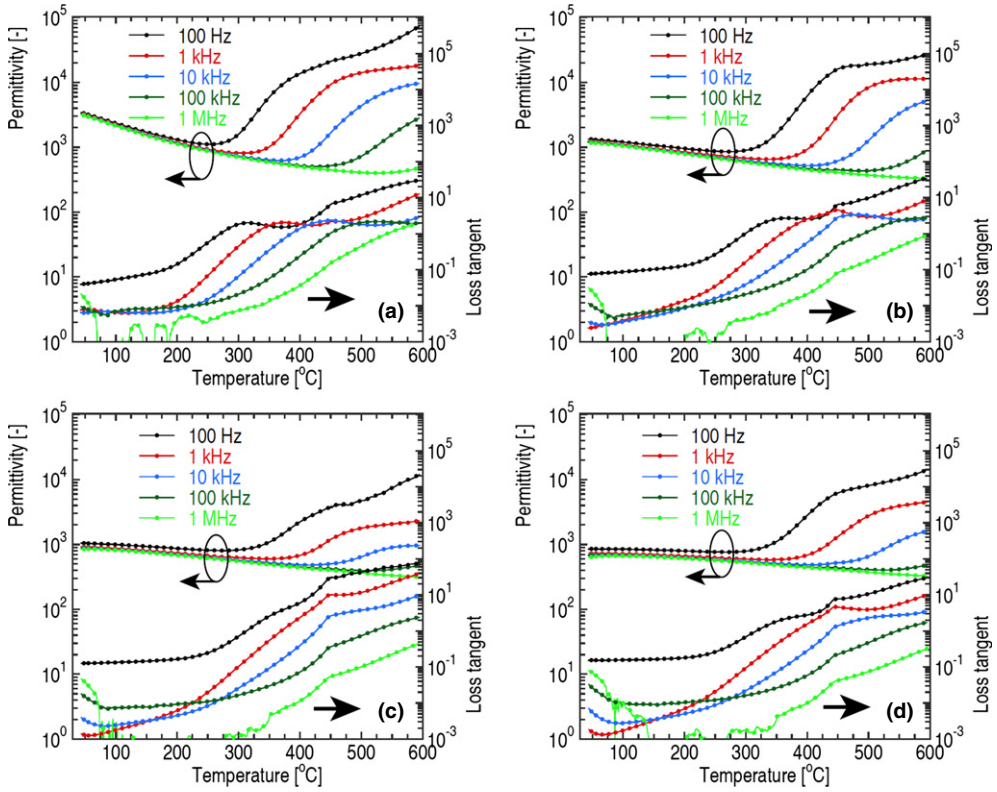

Fig. 5. Temperature dependence of permittivity and loss of (a) BTBMN1; (b) BTBMN2; (c) BTBMN3; and (d) BTBMN4 ceramics measured from ambient temperature to 600°C.

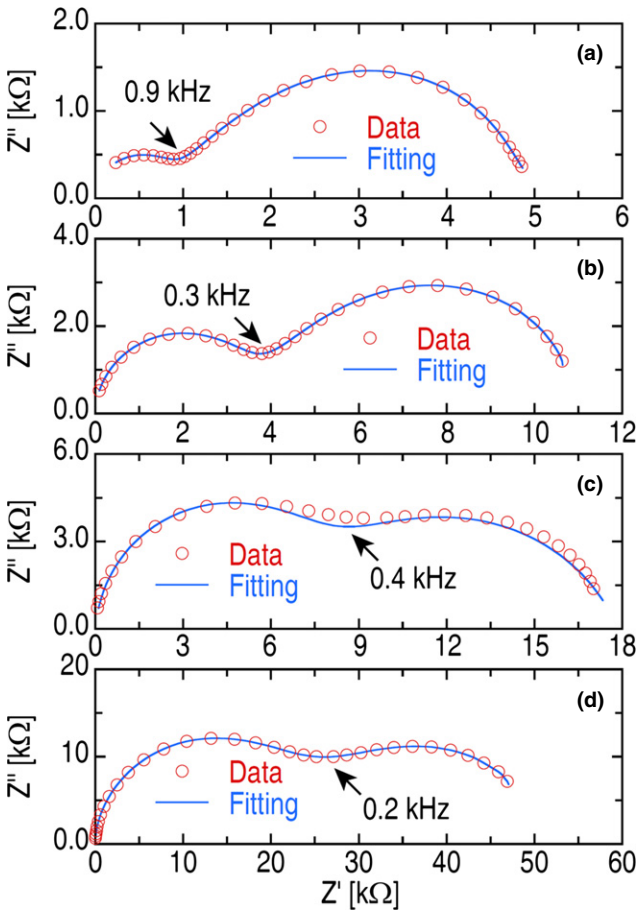

Fig. 6. Complex plane plot of Z″ vs Z′ measured at 500°C of (a) BTBMN1; (b) BTBMN2; (c) BTBMN3; and (d) BTBMN4 ceramics (measured data (red open circles) and fitted (blue line)).

coincident with the reports on PMN–BMN and PT–BMN system.[34,55,56] In addition, the permittivity of BT–BMN ceramics decrease with increasing BMN content is another reason for the improvement of BDS. There is an experimental relationship exists between BDS and permittivity (ε'). McPherson developed a model that BDS should show an approximate $(\varepsilon')^{-1/2}$ dependence over a wide range of high permittivity materials.[57]

Table III shows the result of DC resistivity in BT–BMN ceramics. The resistivity of BT–BMN ceramics increased with increasing BMN at low content, and showed a maximum at $x = 0.15$. BTBMN3 shows high electrical resistivity of 1.53×10^{13} Ω cm. The result was in consistence with the BDS of BT–BMN ceramics. The high resistivity and BDS demonstrate that BT–BMN ceramics have good insulating properties.

The energy storage behavior of the BT–BMN ceramics with different BMN content was investigated by the *P*–*E* hysteresis loops. The *P*–*E* hysteresis loops for all the samples were shown in Fig. 8. Square hysteresis loops, which are often observed in normal ferroelectrics, are not observed in these compositions. The disappearance of square hysteresis could come from the relaxor behavior in this composition range. The BT–BMN ceramics with higher BMN content ($x \geq 0.1$) exhibit linear *P*–*E* relationships. In general, the polarization values of BT–BMN ceramics are decreased effectively by addition of BMN. The energy storage density (*J*) could be calculated according to the equation below:[1]

$$J = \int E \mathrm{d}P \tag{3}$$

where *E* is the applied electric field and *P* is polarization. Figure 9(a) illustrates the energy storage density of BT–BMN ceramics. The energy storage density of BT–BMN ceramics increases with increasing electric field. The charged energy density (J_c) of a dielectric material is equal to the integral of

an area enclosed by charge curve and y-axis. The discharged energy density (J_d) is calculated by integrating the area enclosed by discharge curve and y-axis.[49] The highest charged energy density of 1.13 J/cm^3 was obtained under a high electric field (143.5 kV/cm). As a parameter to evaluate the energy storage property, the energy loss density is as important as the discharged energy density. The energy loss density is defined as the difference between charged and discharged energy densities, quantitatively equal to the inner space of P–E loop. The ambient temperature energy loss densities of studied samples as a function of electric field are presented in Fig. 9(b). All the samples exhibited energy loss densities of less than 0.05 J/cm^3 at the electric field of 143.5 kV/cm, except BTBMN1. With the increase in the BMN content, the energy loss densities of BTBMN ceramics decreased over the entire electric field range. Energy storage, energy loss, and energy release density of BT–BMN ceramics were calculated from the unipolar P–E hysteresis loops as described in Eq. (3), and listed in Table IV. Figure 9(c) illustrates the values of energy storage efficiency (J_d/J_c) for the BT–BMN ceramics.[42] The energy storage efficiency of the BT–BMN ceramics was up to 90%, except BTBMN1. The BTBMN2–4 ceramics possess weak electric field dependences of the energy storage efficiency. The energy storage efficiency

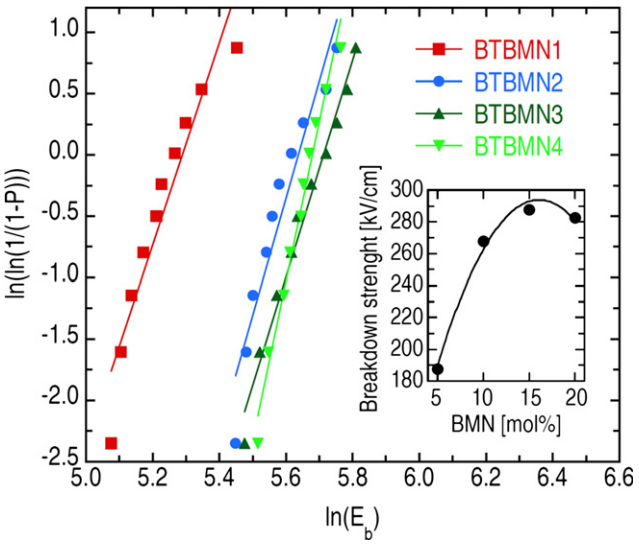

Fig. 7. Weibull distribution of BDS for BT–BMN ceramics with different BMN contents. The Weibull modules are 8.23 (BTBMN1), 9.56 (BTBMN2), 13 (BTBMN3), and 8.86 (BTBMN4), respectively. The inset shows the BDS as a function of the BMN content for BT–BMN ceramics. The thicknesses of specimens are from 0.3 to 0.5 mm. Measurements are carried out in silicon oil with a dc voltage ramp of 1 kV/s until dielectric breakdown occurs.

Table III. Resistivity of BT–BMN Ceramics Measured at Room Temperature

Sample	BTBMN1	BTBMN2	BTBMN3	BTBMN4
Resistivity (Ω·cm)	1.94×10^{12}	1.32×10^{13}	1.53×10^{13}	7.41×10^{12}

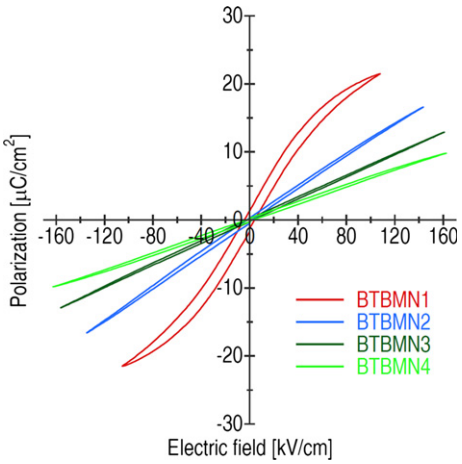

Fig. 8. P–E hysteresis loops of BT–BMN ceramics measured at ambient temperature with a triangular wave form at 10 Hz.

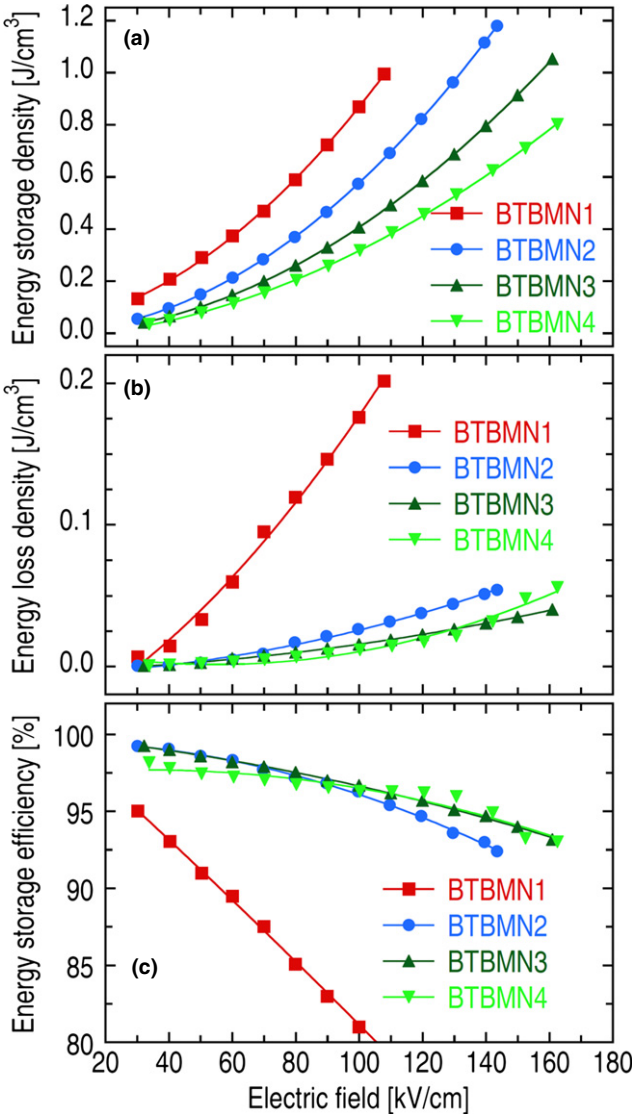

Fig. 9. Ambient temperature (a) energy storage density; (b) energy loss density; and (c) energy storage efficiency versus electric field of BT–BMN ceramics.

Table IV. Energy Storage, Energy Loss, and Energy Release Density of BT–BMN Ceramics

Samples	Energy storage (J/cm^3)	Energy loss (J/cm^3)	Energy release (J/cm^3)
BTBMN1	0.99	0.21	0.79
BTBMN2	1.18	0.05	1.13
BTBMN3	1.05	0.04	1.01
BTBMN4	0.80	0.06	0.74

of the BT–BMN ceramics decreases with increasing electric field, which originates from a dramatic increase in the energy loss density [Fig. 9(b)]. The BTBMN2-4 ceramics exhibit a steady dependence of the energy storage efficiency on the electric field. A slight change appears between 30 and 160 kV/cm. Small variation in the energy storage efficiency is benefit for the utilization of ceramic capacitors in a wider field range.

IV. Conclusions

The $(1-x)BaTiO_3$–$xBi(Mg_{2/3}Nb_{1/3})O_3$ (x = 0.05–0.2) were synthesized by conventional solid-state method. The addition of BMN is favorable for lower sintering temperature. Dielectric measurements revealed a relaxor-like characteristic of BT–BMN ceramics. The permittivity peak of the solid solution ceramics becomes broad and T_m decreases with increasing BMN content. The Weibull factor of BDS indicates the BMN addition can increase the breakdown filed as well as the energy storage density. A highest energy storage density of 1.13 J/cm^3 suggests that the BT–BMN system can be considered as potential candidate for energy storage ceramic capacitors.

Acknowledgments

This work was supported by the National Nature Science Foundation of China (grant no. 51202183), the Fundamental Research Funds for the Central Universities, the International Science & Technology Cooperation Program of China (2013DFR50470), and "111" project (B14040). The SEM work was carried out at International Center for Dielectric Research (ICDR), Xi'an Jiaotong University, Xi'an, China. The authors also thank Mr. Yongyong Zhuang for his help in using SEM.

References

[1]H. Ogihara, C. A. Randall, and S. Trolier-McKinstry, "High-Energy Density Capacitors Utilizing 0.7 $BaTiO_3$-0.3 $BiScO_3$ Ceramics," *J. Am. Ceram. Soc.*, **92**, 1719–24 (2009).

[2]W. Wei, H. Yan, T. Wang, Q. Hu, G. Viola, S. Grasso, Q. Jiang, L. Jin, Z. Xu, and M. J. Reece, "Reverse Boundary Layer Capacitor Model in Glass/Ceramic Composites for Energy Storage Applications," *J. Appl. Phys.*, **113**, 024103, 5pp (2013).

[3]A. Toprak and O. Tigli, "Piezoelectric Energy Harvesting: State-of-the-Art and Challenges," *Appl. Phys. Rev.*, **1**, 031104, 14pp (2014).

[4]N. H. Fletcher, A. D. Hilton, and B. W. Ricketts, "Optimization of Energy Storage Density in Ceramic Capacitors," *J. Phys. D: Appl. Phys.*, **29**, 253–8 (1996).

[5]I. Burn and D. M. Smyth, "Energy Storage in Ceramic Dielectrics," *J. Mater. Sci.*, **7**, 339–43 (1972).

[6]G. R. Love, "Energy Storage in Ceramic Dielectrics," *J. Am. Ceram. Soc.*, **73**, 323–8 (1990).

[7]X. Hao, "A Review on the Dielectric Materials for High Energy-Storage Application," *J. Adv. Dielect.*, **3**, 1330001, 14pp (2013).

[8]H. Lee, J. R. Kim, M. J. Lanagan, S. Trolier-McKinstry, and C. A. Randall, "High-Energy Density Dielectrics and Capacitors for Elevated Temperatures: $Ca(Zr,Ti)O_3$," *J. Am. Ceram. Soc.*, **96**, 1209–13 (2013).

[9]D. P. Shay, N. J. Podraza, N. J. Donnelly, and C. A. Randall, "High Energy Density, High Temperature Capacitors Utilizing Mn-Doped 0.8$CaTiO_3$-0.2$CaHfO_3$ Ceramics," *J. Am. Ceram. Soc.*, **95**, 1348–55 (2012).

[10]X. Wang, Y. Zhang, X. Song, Z. Yuan, T. Ma, Q. Zhang, C. Deng, and T. Liang, "Glass Additive in Barium Titanate Ceramics and Its Influence on Electrical Breakdown Strength in Relation with Energy Storage Properties," *J. Eur. Ceram. Soc.*, **32**, 559–67 (2012).

[11]X. Hao, J. Zhai, and X. Yao, "Improved Energy Storage Performance and Fatigue Endurance of Sr-Doped $PbZrO_3$ Antiferroelectric Thin Films," *J. Am. Ceram. Soc.*, **92**, 1133–5 (2009).

[12]M. Ye, Q. Sun, X. Chen, Z. Jiang, and F. Wang, "Effect of Eu Doping on the Electrical Properties and Energy Storage Performance of $PbZrO_3$ Antiferroelectric Thin Films," *J. Am. Ceram. Soc.*, **95**, 1486–8 (2012).

[13]B. Ma, D.-K. Kwon, M. Narayanan, and U. Balachandran, "Fabrication of Antiferroelectric PLZT Films on Metal Foils," *Mater. Res. Bull.*, **44**, 11–4 (2009).

[14]B. Ma, D.-K. Kwon, M. Narayanan, and U. Balachandran, "Dielectric Properties and Energy Storage Capability of Antiferroelectric $Pb_{0.92}La_{0.08}Zr_{0.95}Ti_{0.05}O_3$ Film-on-Foil Capacitors," *J. Mater. Res.*, **24**, 2993–6 (2009).

[15]X. Hao, Z. Yue, J. Xu, S. An, and C. Nan, "Energy Storage Performance and Electrocaloric Effect in (100)-Preferred $Pb_{0.97}La_{0.02}(Zr_{0.95}Ti_{0.05})O_3$ Antiferroelectric Thick Films," *J. Appl. Phys.*, **110**, 064109, 5pp (2011).

[16]D. Damjanovic, D. Klein, J. Li, and V. Porokhonskyy, "What Can Be Expected from Lead-Free Piezoelectric Materials?" *Funct. Mater. Lett.*, **3**, 5–13 (2010).

[17]F. Gao, X. Dong, C. Mao, F. Cao, and G. Wang, "C/a Ratio-Dependent Energy-Storage Density in $(0.9-x)Bi_{0.5}Na_{0.5}TiO_3$-$XBaTiO_3$-$0.1K_{0.5}Na_{0.5}NbO_3$ Ceramics," *J. Am. Ceram. Soc.*, **94**, 4162–4 (2011).

[18]F. Gao, X. Dong, C. Mao, W. Liu, H. Zhang, L. Yang, F. Cao, and G. Wang, "Energy-Storage Properties of $0.89Bi_{0.5}Na_{0.5}TiO_3$-$0.06BaTiO_3$-$0.05K_{0.5}Na_{0.5}NbO_3$ Lead-Free Anti-Ferroelectric Ceramics," *J. Am. Ceram. Soc.*, **94**, 4382–6 (2011).

[19]L. Jin, F. Li, and S. Zhang, "Decoding the Fingerprint of Ferroelectric Loops: Comprehension of the Material Properties and Structures," *J. Am. Ceram. Soc.*, **97**, 1–27 (2014).

[20]L. E. Cross, "Relaxor Ferroelectric," *Ferroelectrics*, **76**, 241–67 (1987).

[21]N. de Mathan, E. Husson, G. Calverin, and A. Morell, "Structural Study of A Poled $PbMg_{1/2}Nb_{2/3}O_3$ Ceramic at Low-Temperature," *Mater. Res. Bull.*, **26**, 1167–72 (1991).

[22]J. Kuwata, K. Uchino, and S. Nomura, "Diffuse Phase-Transition in Lead Zinc Niobate," *Ferroelectrics*, **22**, 863–7 (1979).

[23]F. Li, L. Jin, Z. Xu, and S. Zhang, "Electrostrictive Effect in Ferroelectrics: An Alternative Approach to Improve Piezoelectricity," *Appl. Phys. Rev.*, **1**, 011103, 21pp (2014).

[24]H. Ogihara, C. A. Randall, and S. Trolier-McKinstry, "Weakly Coupled Relaxor Behavior of $BaTiO_3$–$BiScO_3$ Ceramics," *J. Am. Ceram. Soc.*, **92**, 110–8 (2009).

[25]N. Triamnak, R. Yimnirun, J. Pokorny, and D. P. Cann, "Relaxor Characteristics of the Phase Transformation in $(1-x)BaTiO_3$-$xBi(Zn_{1/2}Ti_{1/2})O_3$ Perovskite Ceramics," *J. Am. Ceram. Soc.*, **96**, 3176–82 (2013).

[26]Q. Zhang, Z. Li, F. Li, and Z. Xu, "Structural and Dielectric Properties of $Bi(Mg_{1/2}Ti_{1/2})O_3$-$BaTiO_3$ Lead-Free Ceramics," *J. Am. Ceram. Soc.*, **94**, 4335–9 (2011).

[27]H. Arvind, K. Umesh, R. E. Newnham, and L. E. Cross, "Stabilization of the Perovskite Phase and Dielectric Properties of Ceramics in the $Pb(Zn_{1/3}Nb_{2/3})O_3$-$BaTiO_3$ System," *Am. Ceram. Soc. Bull.*, **66**, 671–6 (1987).

[28]Z. Li, Q. Li, L. Zhang, and X. Yao, "Dielectric Properties and Transition Temperature of Ceramics in the $Pb(Mg_{1/3}Nb_{2/3})O_3$-$BaTiO_3$ System," *Ferroelectrics*, **262**, 47–52 (2001).

[29]C. C. Huang and D. P. Cann, "Phase Transitions and Dielectric Properties in $Bi(Zn_{1/2}Ti_{1/2})O_3$-$BaTiO_3$ Perovskite Solid Solutions," *J. Appl. Phys.*, **104**, 024117, 4pp (2008).

[30]N. Raengthon and D. P. Cann, "Dielectric Relaxation in $BaTiO_3$-$Bi(Zn_{1/2}Ti_{1/2})O_3$ Ceramics," *J. Am. Ceram. Soc.*, **95**, 1604–12 (2011).

[31]X. Wang and A. Yang, "Dielectric and Ferroelectric Properties of $(Bi_xBa_{1-x})(Zn_{x/2}Ti_{1-x/2})O_3$ Ceramics," *J. Phys. D: Appl. Phys.*, **42**, 075419, 7pp (2009).

[32]D. H. Choi, A. Baker, M. Lanagan, S. Trolier-McKinstry, and C. A. Randall, "Structural and Dielectric Properties in $(1-x)BaTiO_3$-$xBi(Mg_{1/2}Ti_{1/2})O_3$ Ceramics ($0.1 \le x \le 0.5$) and Potential for High-Voltage Multilayer Capacitors," *J. Am. Ceram. Soc.*, **96**, 2197–202 (2013).

[33]D.-K. Kwon and M. H. Lee, "Temperature-Stable High-Energy-Density Capacitors Using Complex Perovskite Thin Films," *IEEE Trans. Ultrason. Ferroelectr. Freq. Control*, **59**, 1894–9 (2012).

[34]L. Hong, L.-Y. Zhao, X.-W. Zhu, L.-Y. Zheng, J.-T. Zeng, and G.-R. Li, "Properties and Phase-Transition Temperature of $(1-x)Bi(Mg_{2/3}Nb_{1/3})O_3$-$XPbTiO_3$ Piezoelectric Ceramics Near the Morphotropic Phase Boundary," *J. Inorg. Mater.*, **27**, 735–40 (2012).

[35]J. Zhao, H. Du, S. Qu, J. Wang, H. Zhang, Y. Yang, and Z. Xu, "The Effects of $Bi(Mg_{2/3}Nb_{1/3})O_3$ on Piezoelectric and Ferroelectric Properties of $K_{0.5}Na_{0.5}NbO_3$ Lead-Free Piezoelectric Ceramics," *J. Alloys Compd*, **509**, 3537–40 (2011).

[36]P. D. Spagnol, J. A. Varela, M. A. Zaghete, E. Longo, and S. M. Tebcherani, "Evidence of Hetero-Epitaxial Growth of $Pb(Mg_{1/3}Nb_{2/3})O_3$ on the $BaTiO_3$ Seed Particles of a Citrate Solution," *Mater. Chem. Phys.*, **77**, 918–23 (2002).

[37]N. Setter and L. E. Cross, "The Contribution of Structural Disorder to Diffuse Phase Transitions in Ferroelectrics," *J. Mater. Sci.*, **15**, 2478–82 (1980).

[38]A. A. Bokov and Z. G. Ye, "Recent Progress in Relaxor Ferroelectrics with Perovskite Structure," *J. Mater. Sci.*, **41**, 31–52 (2006).

[39]S. Anwar, P. R. Sagdeo, and N. P. Lalla, "Ferroelectric Relaxor Behavior in Hafnium Doped Barium-Titanate Ceramic," *Solid State Commun.*, **138**, 331–6 (2006).

[40]M. Li, D. C. Sinclair, and A. R. West, "Extrinsic Origins of the Apparent Relaxorlike Behavior in $CaCu_3Ti_4O_{12}$ Ceramics at High Temperatures: A Cautionary Tale," *J. Appl. Phys.*, **109**, 084106, 9pp (2011).

[41]C. Li and X. Wei, "Complex Impedance Analysis on a Layered Perovskite-Like Ceramic: $La_3Ti_2TaO_{11}$," *J. Mater. Sci.*, **47**, 4200–4 (2012).

[42]M. Li, A. Feteira, and D. C. Sinclair, "Relaxor Ferroelectric-Like High Effective Permittivity in Leaky Dielectrics/Oxide Semiconductors Induced by Electrode Effects: A Case Study of CuO Ceramics," *J. Appl. Phys.*, **105**, 114109, 8pp (2009).

[43]S. H. Yoon, C. A. Randall, and K. H. Hury, "Effect of Acceptor (Mg) Concentration on the Resistance Degradation Behavior in Acceptor (Mg)-Doped $BaTiO_3$ Bulk Ceramics: I. Impedance Analysis," *J. Am. Ceram. Soc.*, **92**, 1758–65 (2009).

[44]M. Li, A. Feteira, M. Mirsaneh, S. Lee, M. T. Lanagan, C. A. Randall, and D. C. Sinclair, "Influence of Nonstoichiometry on Extrinsic Electrical Conduction and Microwave Dielectric Loss of $BaCo_{1/3}Nb_{2/3}O_3$ Ceramics," *J. Am. Ceram. Soc.*, **93**, 4087–95 (2010).

[45]J. T. S. Irvine, D. C. Sinclair, and A. R. West, "Electroceramics: Characterization by Impedance Spectroscopy," *Adv. Mater.*, **2**, 132–8 (1990).

[46]W. Weibull, "A Statistical Distribution Function of Wide Applicability," *J. Appl. Mech.*, **18**, 293–7 (1951).
[47]E. Tuncer, D. R. James, I. Sauers, A. R. Ellis, and M. O. Pace, "On Dielectric Breakdown Statistics," *J. Phys. D: Appl. Phys.*, **39**, 4257–68 (2006).
[48]J. Huang, Y. Zhang, T. Ma, H. Li, and L. Zhang, "Correlation Between Dielectric Breakdown Strength and Interface Polarization in Barium Strontium Titanate Glass Ceramics," *Appl. Phys. Lett.*, **96**, 042902, 3pp (2010).
[49]T. Wang, X. Wei, Q. Hu, L. Jin, Z. Xu, and Y. Feng, "Effects of $ZnNb_2O_6$ Addition on $BaTiO_3$ Ceramics for Energy Storage," *Mater. Sci. Eng., B*, **178**, 1081–6 (2013).
[50]T. Wang, L. Jin, L. Shu, Q. Hu, and X. Wei, "Energy Storage Properties in $Ba_{0.4}Sr_{0.6}TiO_3$ Ceramics with Addition of Semi-Conductive $BaO–B_2O_3–SiO_2–Na_2CO_3–K_2CO_3$ Glass," *J. Alloys. Comp.*, **617**, 399–403 (2014).
[51]T. Wang, L. Jin, Y. Tian, L. Shu, Q. Hu, and X. Wei, "Microstructure and Ferroelectric Properties of Nb_2O_5-Modified $BiFeO_3$-$BaTiO_3$ Lead-Free Ceramics for Energy Storage," *Mater. Lett.*, **137**, 79–81 (2014).
[52]Z. H. Wu, H. X. Liu, M. H. Cao, Z. Y. Shen, Z. H. Yao, H. Hao, and D. B. Luo, "Effect of BaO-Al_2O_3-B_2O_3-SiO_2 Glass Additive on Densification and Dielectric Properties of $Ba_{0.3}Sr_{0.7}TiO_3$ Ceramics," *J. Ceram. Soc. Jpn.*, **116**, 345–9 (2008).
[53]Y. Li, H. Liu, Z. Yao, J. Xu, Y. Cui, H. Hao, M. Cao, and Z. Yu, "Characterization and Energy Storage Density of $BaTiO_3$-$Ba(Mg_{1/3}Nb_{2/3})O_3$ Ceramics," *Mater. Sci. Forum*, **654–656**, 2045–8 (2010).
[54]Y. Li, G. Dong, Q. Liu, and D. Wu, "Preparation and Investigation on Properties of BST-Base Ceramic with High-Energy Storage Density," *J. Adv. Dielect.*, **3**, 1350005, 5pp (2013).
[55]Y. S. Kim and N. K. Kim, "Dielectric Characteristics of Bismuth-Modified Lead Magnesium Niobate Ceramics," *Mater. Res. Bull.*, **39**, 1177–83 (2004).
[56]R. Wanga, Y. Shimojoa, T. Sekiyaa, and M. Itoh, "Predominant Factors Affecting the Dielectric and Piezoelectric Properties of Bismuth-Containing Complex Perovskite Solid Solution," *Solid State Commun.*, **134**, 791–5 (2005).
[57]J. McPherson, J. Y. Kim, A. Shanware, and H. Mogul, "Thermochemical Description of Dielectric Breakdown in High Dielectric Constant Materials," *Appl. Phys. Lett.*, **82**, 2121–3 (2003). □